

Broadband Circularly Polarized Microstrip Patch Antenna Using Circular Artificial Ground Structure and Meandering Probe

KHANET POOKKAPUND¹, (Member, IEEE),
ARNON SAKONKANAPONG¹, (Student Member, IEEE),
RYUJI KUSE², (Member, IEEE), CHUWONG PHONGCHAROENPANICH¹, (Member, IEEE),
AND TAKESHI FUKUSAKO², (Senior Member, IEEE)

¹Faculty of Engineering, King Mongkut's Institute of Technology Ladkrabang, Bangkok 10520, Thailand

²Faculty of Advanced Science and Technology, Kumamoto University, Kumamoto 860-8555, Japan

Corresponding author: Chuwong Phongcharoenpanich (chuwong.ph@kmitl.ac.th)


ABSTRACT To enhance axial ratio (AR) bandwidth, this research proposes a circularly polarized (CP) single-fed microstrip patch antenna using a circular artificial ground structure (AGS) and meandering probe. To achieve broader AR bandwidth, the circular AGS is populated with rectangular unit cells and partially cut unit cells along the circular contour, while the meandering probe is used to improve the impedance bandwidth. Simulations are performed and results compared with that of conventional rectangular-AGS antenna. The simulation results show that the circular-AGS antenna, given 62 mm circular ground plane, achieves broader impedance (5.12 - 9.00 GHz and 54%), AR (5.21 - 8.27 GHz and 45%) and gain bandwidths (3.85 - 7.00 GHz and 58.06%), in comparison with the rectangular-AGS antenna (4.50 - 7.45 GHz and 49%; 4.52 - 7.42 GHz and 21%; and 4.00 - 6.80 GHz and 51.58% for impedance, AR and gain bandwidths). The circular-AGS antenna is capable of converting linear polarization in the off-axial ratio band into circular polarization. To verify, a circular-AGS antenna prototype is fabricated and experiments undertaken. The experimental impedance, AR and gain bandwidths of the circular-AGS antenna are 47.82% (5.17 - 8.42 GHz), 43.81% (5.24 - 8.17 GHz) and 60.74% (3.75 - 7.00 GHz). The proposed circular-AGS antenna can achieve broader AR bandwidth and is thus ideal for broadband CP applications. The novelty of this research lies in the use of circular AGS to effectively enhance AR bandwidth, as opposed to rectangular AGS which is conventionally used in CP polarizers.

INDEX TERMS Artificial ground structure (AGS), artificial magnetic conductor, broadband antenna, circular polarization, microstrip patch antenna.

I. INTRODUCTION

Circularly polarized (CP) antennas are utilized in wireless devices and systems to mitigate polarization loss, such as wireless local area network (WLAN), radio frequency identification (RFID), and satellite telecommunications [1].

A number of techniques have been proposed for single-fed broadband CP antennas, including tapered microstrip feed with L-shaped slits [2], single-fed parasitic patches [3], sequential-phase feed with shorted loop [4], stacked corner-truncated patches [5], and a microstrip-fed slot antenna with split ring resonators [6]. In addition, coupling feed [7], [8],

The associate editor coordinating the review of this manuscript and approving it for publication was Jaime Laviada .

multi-layers [9], coplanar waveguide feed [10], air gap [11], and cavity-backed structures [12]–[14] are utilized in realization of broadband circular polarization. Despite enhanced antenna bandwidth, the aforementioned antennas suffer from bulkiness.

As a result, artificial magnetic conductors (AMC) are used to realize wide impedance bandwidth with low-profile structure because the radiating patch could be positioned in close proximity to the AMC with a distance less than a quarter-wavelength. In practice, AMC could be employed to achieve circular polarization [15], [16]. Specifically, the impedance and AR bandwidths of 36% and 33% are achieved with AMC as backed reflector [17]. In [18]–[20], AMC is positioned above the radiating patch to realize CP radiation with AR

bandwidth of 23% and 28%, respectively. Dipoles and bowtie elements are positioned above AMC to achieve dual-band CP with the lower and higher bandwidths of 19% and 34%, but the antenna height is more than a quarter-wavelength [21].

In addition, complementary split-ring resonator (CSR) with AMC ground plane [22] and complementary cross-bar fractal tree (CCFT) and three-turn complementary spiral resonators (TCSRs) with reactive impedance surface (RIS) ground plane [23] are utilized to tackle the antenna bulkiness. However, the techniques suffer from narrow AR bandwidths. As a result, a single-fed rectangular CP patch antenna with truncated corners and rectangular artificial ground structure (AGS) populated with rectangular-shaped unit cells is proposed to enhance AR bandwidth [24]. In [25], the AMC-based AGS could convert linear polarization in the off-axial ratio band ($AR > 3\text{dB}$) into circular polarization and achieve broader AR bandwidth in higher frequency. Besides, the AR bandwidth is enhanced by varying the ground plane diameter, achieving an AR bandwidth of 30% [26].

To address the antenna bulkiness and enhance the AR bandwidth, this research proposes a CP single-fed microstrip patch antenna using a circular AGS structure and meandering probe on the circular ground plane. The circular AGS is deployed to enhance the AR bandwidth and the meandering probe to improve the impedance bandwidth. In [27]–[29], the meandering probe technique is used to improve impedance matching. The radiating patch of the proposed CP microstrip patch antenna is of square shape with diagonally truncated corners, and the circular AGS is populated with rectangular unit cells and partially-cut rectangular unit cells along the circular contour. Simulations are carried out, and an antenna prototype is fabricated and experimented. In addition, the performance of the circular-AGS antenna is compared with that of a rectangular-AGS antenna.

II. ANTENNA CONFIGURATION

Fig. 1 illustrates the geometry of the proposed broadband CP microstrip patch antenna, consisting of corners-truncated square radiating patch, circular AGS, meandering probe, and circular ground plane. The square radiating patch with diagonally truncated corners could independently achieve right-hand circular polarization (RHCP) at 6 GHz. The radiating patch is rotated 45° to the x-axis to generate in-phase electric fields in the x- and y-directions. The radiating patch sits on Rogers RT/Duroid 5880 substrate of 1.6 mm in thickness and 62 mm in diameter (upper layer).

Figure 2 illustrates the cross-sectional view of the meandering probe, consisting of upper and lower arms and shorter and taller vias. The SMA connector is driving the meandered line, which is exciting the antenna using a via. Two unit cells at the center of the circular AGS are removed to accommodate the upper arm of the meandering probe. The current on the upper and lower arms flow in the opposite direction, and so do the current on the vias. The phenomenon suppresses cross-polarization of the antenna [27]–[29]. A fan stub is incorporated for broadband impedance matching.

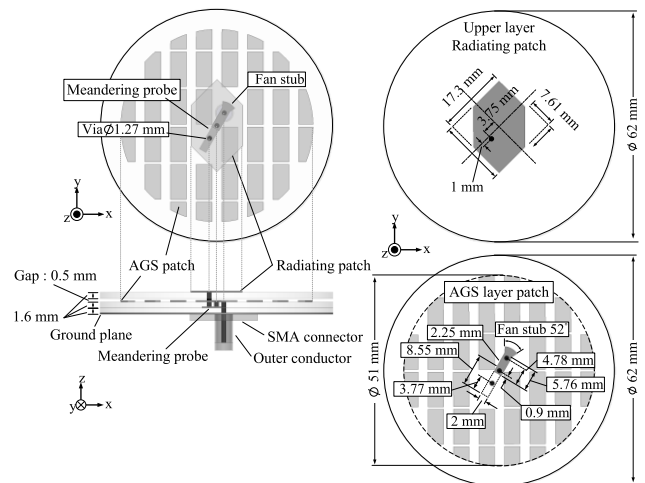


FIGURE 1. Geometry of the proposed broadband CP microstrip patch antenna.

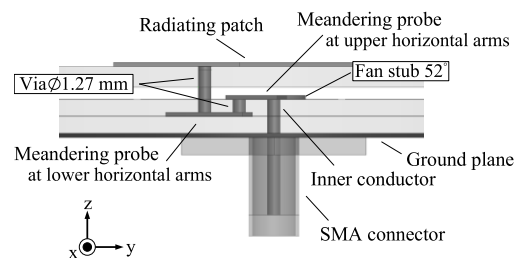


FIGURE 2. Cross-sectional view of the meandering probe consisting of upper and lower arms and shorter and taller vias.

The width and length of the upper arm are 2.25 mm and 5.76 mm, and those of the lower arm are 2 mm and 8.55 mm. The fan stub with a radius of 4.2 mm and flare of 52° is adjoined to one end of the upper arm, with a distance of 1.33 mm from the inner conductor center. The diameter of the vias is 1.27 mm. The meandering probe is underneath the center of the radiating patch and aligned 29.5° to the y-axis for adjusting amplitude ratio of x- and y-components. The feeding point of the radiating patch (i.e., where the radiating patch is connected to the meandering probe) is 3.75 mm and 1 mm from the center of the radiating patch. The offset distance of 1 mm from the diagonal is slightly adjusted for matching impedance.

In addition, there is an air gap of 0.5 mm between the radiating patch and AGS patch to enhance impedance matching. The air gap itself has little effect on characteristics [24]–[25]. In this research, simulations are carried out with two ground-plane diameters: 51 and 62 mm, and the optimal circular ground plane dimension is determined.

III. THE AGS UNIT CELLS AND GROUND PLANE

A. RECTANGULAR AND PARTIALLY-CUT RECTANGULAR UNIT CELLS

Fig. 3 illustrates the geometry of a rectangular unit cell of the circular AGS [24]–[26]. The structure could achieve circular

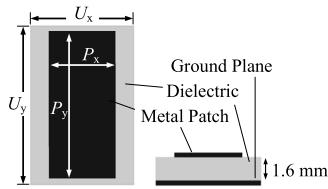


FIGURE 3. Geometry of a rectangular unit cell of the circular AGS.

polarization with $+90^\circ$ and -90° reflection phases for x- and y-polarization. The width (U_x) and length (U_y) of the area encompassing the copper patch and substrate are 6.5 and 10 mm, and the width (P_x) and length (P_y) of the rectangular copper patch (i.e., unit cell) are 4.20 and 9.25 mm [24]–[26].

In [25]–[30], broad CP radiation is achieved by rotating the radiating patch 45° to the x-axis, in conjunction with the rectangular AGS. Specifically, the RHCP is a synthesis of the wave from the radiating patch and the reflected wave from the AGS.

Fig. 4 illustrates the proposed AGS populated with rectangular unit cells (type C) and partially-cut unit cells (types A and B) along the leftmost and rightmost of the circular AGS.

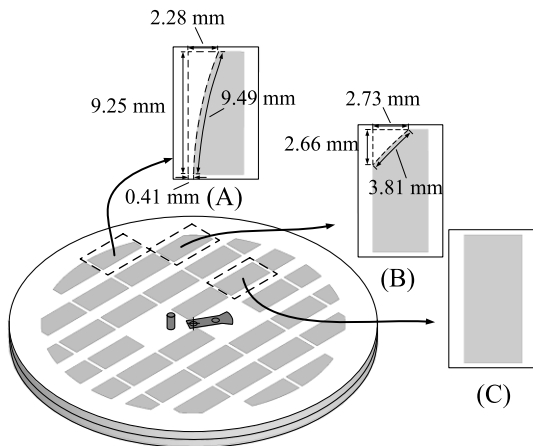


FIGURE 4. Proposed circular AGS with types-A, B, and C unit cells (Antenna#1).

Fig. 5 depicts the simulated reflection phases of x- (E_x) and y-polarization (E_y) of types-A, B, and C unit cells and the phase difference, using Ansoft HFSS version 16.0. The reflection phase difference of 180° is achieved at 7.00 - 7.50 GHz for type-A unit cell, 7.50 - 9.00 GHz for type-B unit cell, and 6.00 - 6.50 GHz for type-C unit cell. As a result, the concurrent use of types-A, B, and C unit cells enhances the AR bandwidth, covering the 6.00 - 9.00 GHz frequency band. E_x is less influenced by the unit cell types, compared to E_y which is noticeably subject to the unit cell types. To achieve the CP ($AR \leq 3\text{dB}$), a phase-difference error between E_x and E_y of 20° is acceptable, given 180° -phase difference [24]–[26].

Figs. 6(a)–(f) respectively illustrate six circular AGS configurations containing types-A, B, and/or C unit cells along

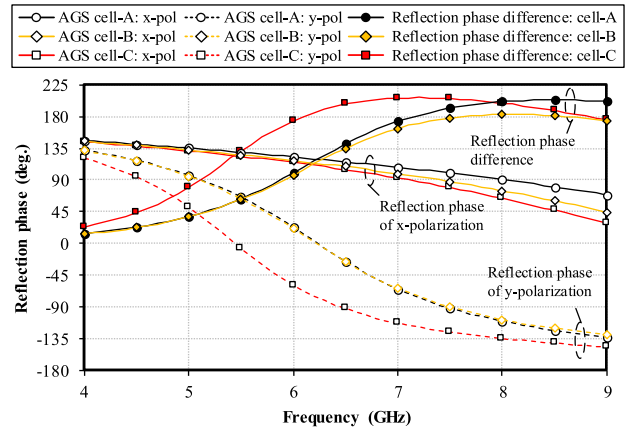


FIGURE 5. Simulated reflection phases of x- and y-polarization and phase difference of types-A, B, and C unit cells.

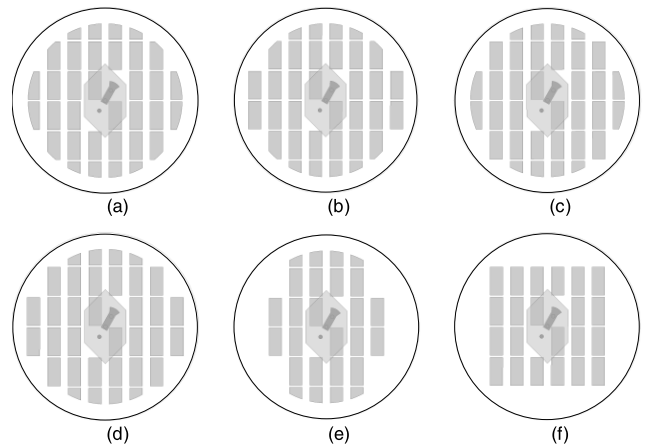


FIGURE 6. AGS configurations containing types-A, B and/or C unit cells: (a) Antenna #1 (proposed structure), (b) Antenna #2, (c) Antenna #3, (d) Antenna #4, (e) Antenna #5, (f) Antenna #6.

the leftmost and rightmost of the circular AGS, given types D and E unit cells (discussed in the subsequent sub-section) in the uppermost and lowermost rows: Antenna #1 (the proposed antenna), Antenna #2 (containing types-B and C unit cells), Antenna #3 (containing types-A and C unit cells), Antenna #4 (containing type-C), Antenna #5 (types-A and B unit cells removed from leftmost and rightmost columns), and Antenna #6 (only type-C with 6×4 planar arrangement). The width of types-A, B, and C unit cells are identical (i.e., 4.20 mm). The number of unit cells for Antennas #1–#4 is 34, whereas those of Antennas #5 and #6 are 26 and 22, respectively.

Figs. 7 and 8 respectively illustrate the simulated AR along the $+z$ direction, amplitude ratio (E_y/E_x), and phase difference ($\angle E_y - \angle E_x$) of Antennas #1–#6. In Fig. 7, the minimum AR point occurred at the lowest frequency was caused by the driven patch. The other minimum AR points at higher frequencies were generated by the surface waves from a number of unit cells. The minimum AR points of Antennas #1–#4 (each antenna contains 34 unit cells) occurred at the

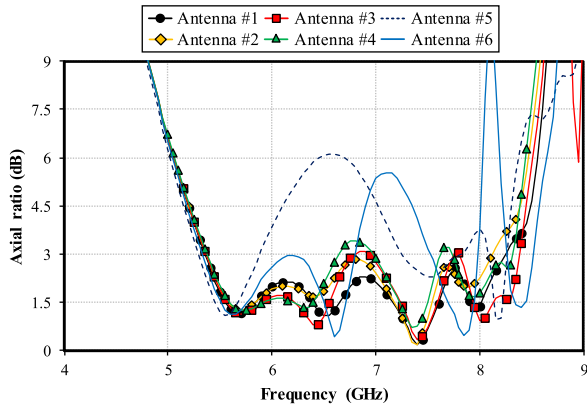


FIGURE 7. Simulated axial ratio of Antennas #1-#6.

similar frequencies, but the levels of minimum AR points are different due to the reflection phase of various types of unit cells from Fig.5. When some unit cells were removed as Antennas #5-#6, the minimum AR point caused by the driven patch slightly moved down, whereas the subsequent AR points were shifted to the higher frequencies. This phenomenon is similar to the antenna studied in [18]. At 7 GHz, AR of Antennas #2-#6 are greater than 3dB (AR>3dB), with E_y/E_x and $\angle E_y - \angle E_x$ deviating from 0 dB and 90° as shown in Fig.8. The simulation results indicate that, at 7 GHz, the concurrent implementation of types-A and B unit cells along the left and right contour of the circular AGS effectively reduces AR (≤ 3 dB), vis-à-vis the rectangular-AGS antenna whose AR is > 3 dB [24], [25].

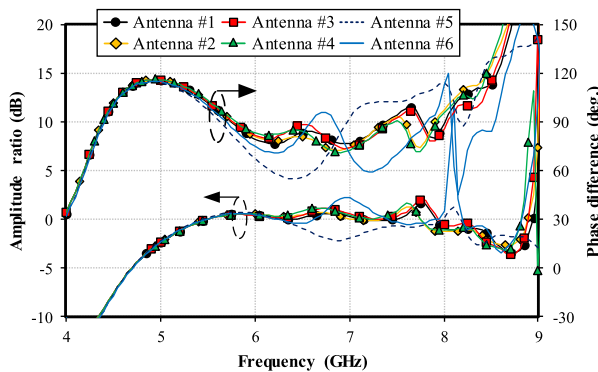


FIGURE 8. Simulated amplitude ratio and phase difference of Antennas #1-#6.

Figs. 9-11 respectively depict the current distribution, at 7 GHz, of Antenna #1 (the proposed structure), Antenna #4 (containing type-C), and Antenna #5 (types-A and B unit cells removed from the leftmost and rightmost columns). The dominant direction of current flow with respect to time (t) is represented by the dark bold arrow.

In Fig. 9 (Antenna #1), the current flow is counterclockwise, generating RHCP along the AGS contour. The amplitude of the current along the contour of Antenna #1 (Fig. 9) is stronger than that of Antenna #4 (Fig. 10). The finding

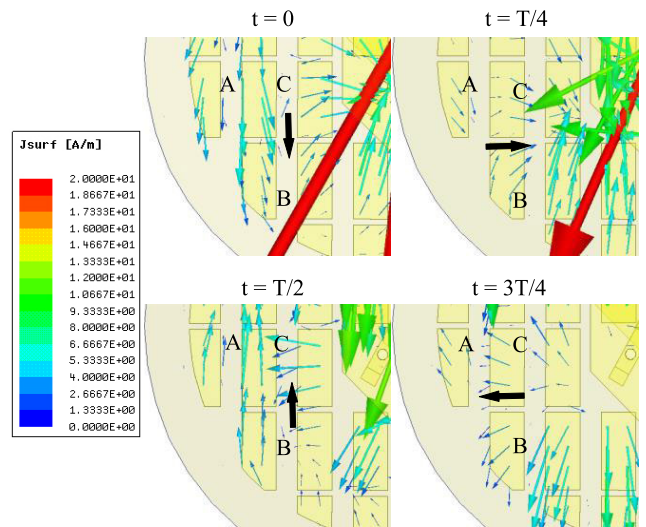


FIGURE 9. Current distribution of the proposed antenna (Antenna #1) in time period T at 7 GHz.

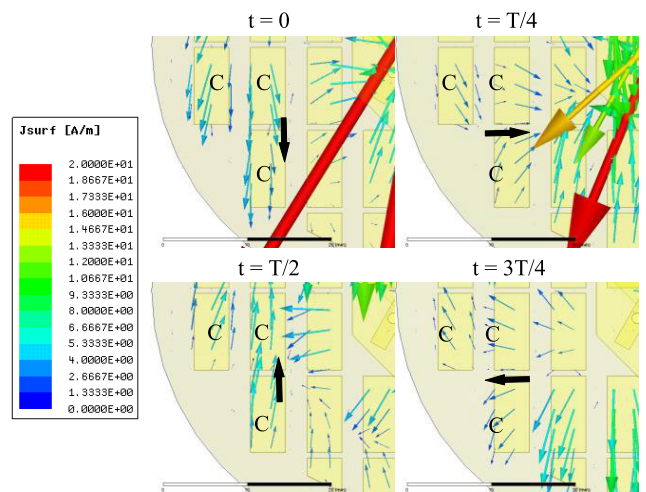


FIGURE 10. Current distribution of Antenna #4 in time period T at 7 GHz.

is attributable to the truncated corners of types-A and B unit cells in the AGS of Antenna #1. The weak amplitude of Antenna #4 results in its amplitude ratio deviating from 0 dB, resulting in large AR (> 3 dB). In Fig. 11 (Antenna #5), the current distribution is of y-direction linear polarization due to the absence of the leftmost and rightmost columns of unit cells. This suggests that the circular polarization could be realized by incorporating types-A and B unit cells into the AGS.

Fig. 12 illustrates the proposed AGS with types-D and E (trapezoid-shaped) unit cells, located at the uppermost and lowermost of the circular AGS. In addition, the shape and dimensions of types-D and E unit cells (Fig. 12) are altered from trapezoid to stunted rectangular shape (i.e., types-D' and E' unit cells) to compare the AR performance. The dimensions of the stunted rectangular-shaped types-D' and E' unit cells are 4.20×2.20 and 4.20×4.55 mm, respectively.

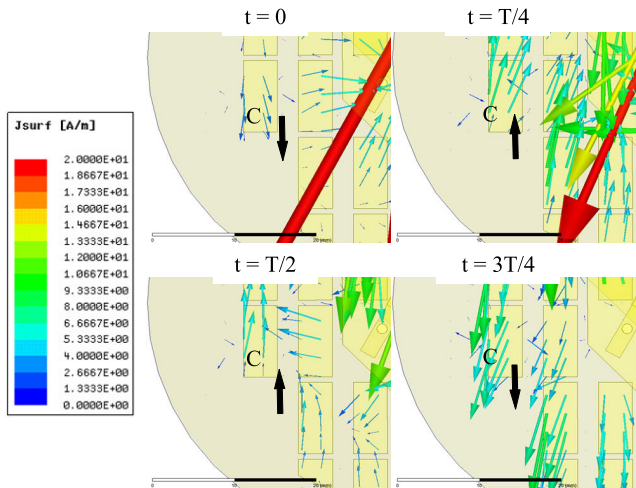


FIGURE 11. Current distribution of Antenna #5 in time period T at 7 GHz.

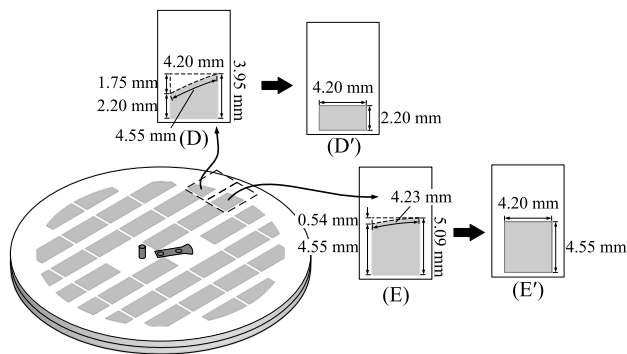


FIGURE 12. Proposed circular AGS with types-D, D', E, and E' unit cells (Antenna #1 structure).

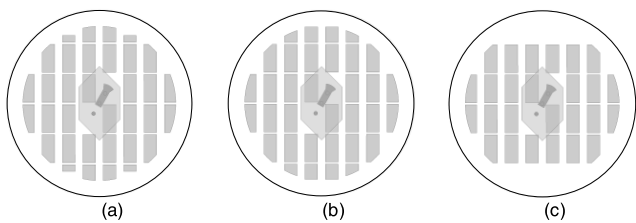


FIGURE 13. AGS configurations containing types-D, D', E, and E' unit cells along the uppermost and lowermost rows of the contour, based on the Antenna #1 structure: (a) Antenna #7, (b) Antenna #8, (c) Antenna #9.

Figs. 13(a)-(c) respectively illustrate three circular AGS configurations populated with types-D, D', E, and E' unit cells along the uppermost and lowermost rows (based on the Antenna #1 structure): Antenna #7 (replacing four type-D unit cells with the same number of type-D'), Antenna #8 (replacing four type-E unit cells with the same number of type-E'), and Antenna #9 (without the uppermost and lowermost rows, i.e., containing no types-D, D', E, and E' unit cells). The width of types-D, D', E, and E' unit cells is identical to that of type-C (i.e., 4.20 mm). The number of unit

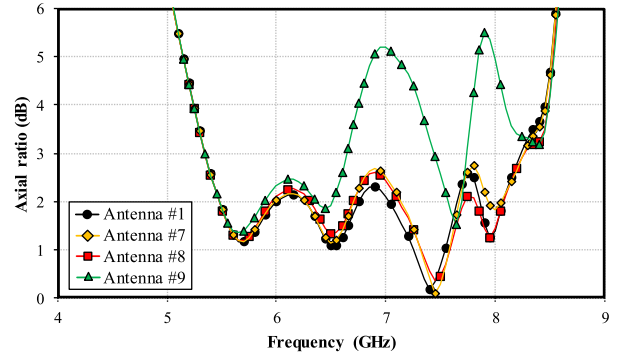


FIGURE 14. Simulated axial ratio of Antennas #1, #7, #8, and #9 relative to frequency.

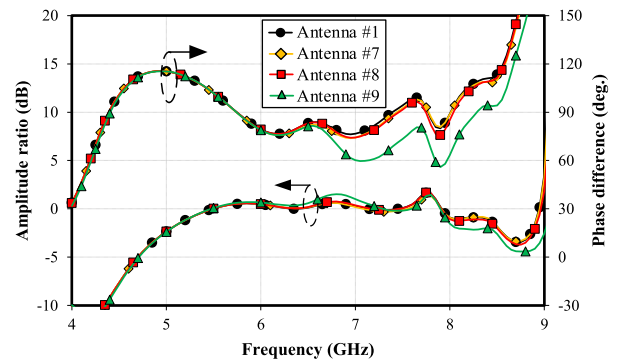


FIGURE 15. Simulated amplitude ratio and phase difference of Antennas #1, #7-#9.

cells for Antennas #7 and #8 are 34, whereas that of Antenna #9 is 26.

Figs. 14 and 15 respectively compares the simulated AR, amplitude ratio (E_y/E_x), and phase difference ($\angle E_y - \angle E_x$) of Antennas #1, #7, #8, and #9 relative to frequency. At 7 GHz, AR of Antennas #1, #7, and #8 are less than 3 dB, indicating right-hand circular polarization. Types-D, D', E, and E' unit cells balance the x- and y-direction current amplitude. Meanwhile, in the absence of types-D, D', E, and E' unit cells, the y-direction current amplitude becomes stronger than that of the x-direction. Antenna #9 exhibits an AR greater than 3 dB because the phase difference is drastically deviated from 90° as shown in Fig.15. The finding suggests that the absence of types-D, D', E, and E' unit cells contributes to non-circular polarization, as shown in Fig. 16. The broadband AR characteristics can be achieved with the combination of minimum AR points from the driven patch and circular AGS with the concurrent use of partially cut unit cells along the circular contour.

B. ENLARGED CIRCULAR GROUND PLANE DIAMETER

Simulations are carried out using Antenna #1 with two ground plane diameters (D): 51 and 62 mm, given the circular AGS diameter of 51 mm. Figs. 17 and 18 respectively illustrate the simulated $|S_{11}|$ and AR in the $+z$ direction, given the two ground plane diameters (D) using Antenna #1.

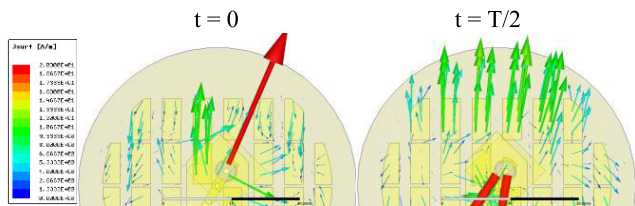


FIGURE 16. Current distribution of Antenna #9 (containing no types-D, D', E, and E' unit cells) in time period T at 7 GHz.

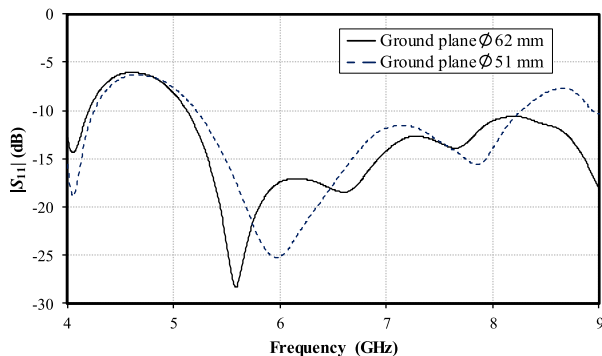


FIGURE 17. Simulated $|S_{11}|$ of different ground plane diameters (51 and 62 mm) using Antenna #1.

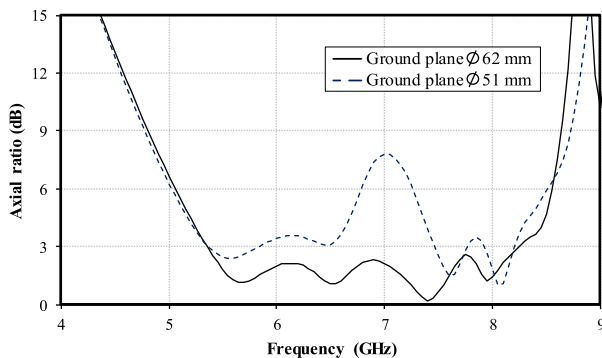


FIGURE 18. Simulated AR in the +z direction different variable ground plane diameters.

At 7 GHz and $D = 51$ mm, AR of the antenna is greater than 3 dB ($>3\text{dB}$) due to the diffractive effects causing the electric field at the edges to spread in both x- and y-directions and subsequently inducing electrical coupling with the adjoining patches. Nevertheless, in [26], at 7 GHz, enlarging the ground plane could improve the AR ($\leq 3\text{dB}$). After expanding the ground plane ($D = 62$ mm), the diffraction at the edges of each element and the interference between diffracted rays from neighbouring elements can be mitigated, and this results in AR improvement.

In light of AR in excess of 3 dB ($\text{AR} > 3\text{dB}$) at 7 GHz for $D = 51$ mm, an optimal circular ground plane diameter (i.e., achieving $\text{AR} \leq 3$ dB at 7 GHz) is determined using eigenvalue analysis and the periodic boundary condition in the high frequency structure simulator (HFSS) with one single type-C unit cell (Fig. 3). Figs. 19(a)-(b) respectively depict

the dispersion diagrams of the AGS in the x- and y-directions given the ground plane of 51 mm, where TE and TM denote transverse electric and transverse magnetic modes. The resonant frequency is calculated by

$$\beta D_0 + \beta' \Delta D = n\pi, \tag{1}$$

where n is an integer, β is a propagation constant (deg/m), β' is a propagation constant in the enlarged substrate and ground plane (deg/m), D_0 is the initial AGS diameter (51 mm).

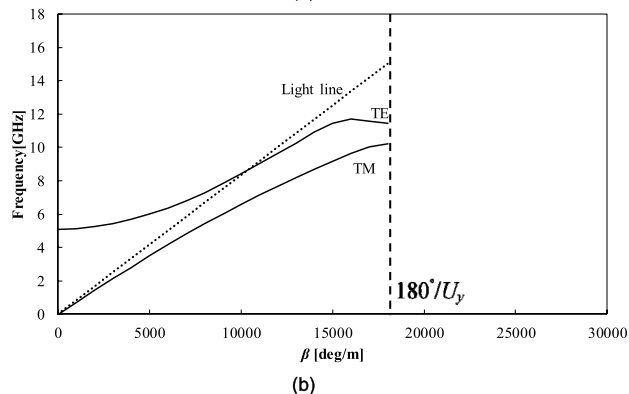
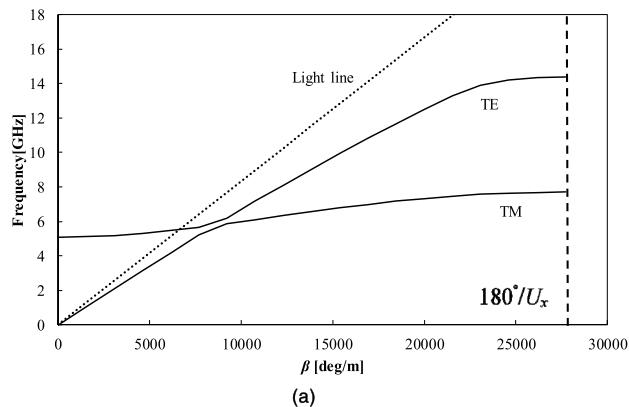


FIGURE 19. Dispersion diagrams of one single type-C unit cell: (a) x-, (b) y-directions.

Table 1 tabulates the resonant frequencies based on Fig. 19 and eq. (1) for $D = 51$ and 62 mm, using the Antenna #1 structure. With $D = 51$ mm, a resonance occurs at 6.91 GHz (TM), consistent with Fig. 18 in which AR peaks around 7 GHz. This is attributable to the current on the circular AGS predominantly flowing in the y-direction. The phenomenon is also observed in Antenna #4 (Fig. 10), Antenna #5 (Fig. 11), and Antenna #9 (Fig. 16).

In Fig. 19(a), given the circular ground plane (D) of 51 mm, TE and TM in the x-direction diverge at higher frequency, as opposed to parallel to each other. The divergence of TE and TM currents induces strong resonance at 7 GHz, as shown in Fig. 18. The enlargement of the circular ground plane dimension (D) from 51 to 62 mm suppresses the resonance, improving the AR ($\leq 3\text{dB}$) (Fig. 18). The optimal circular ground plane diameter is thus 62 mm.

Fig. 20 compares the simulated AR of the non-AGS [25], rectangular-AGS [24]-[25], and circular-AGS antennas,

TABLE 1. TM and TE Mode Resonant Frequencies in The x- and y-directions Given The Ground Plane Diameters (D) of 51 and 62 mm.

D (mm)	51		62	
Resonant frequency (GHz)	TM(x)	TM(y)	TM(x)	TM(y)
	5.59	6.91	6.00	5.84
	7.05	8.75	7.69	7.45

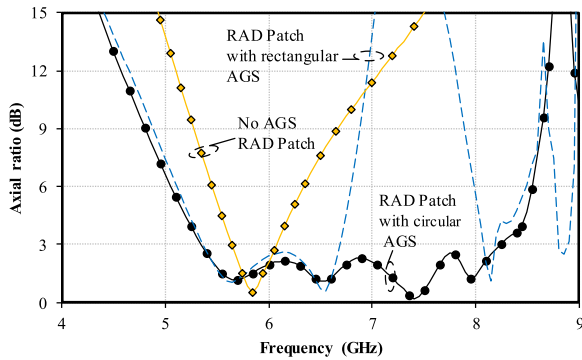


FIGURE 20. Simulated AR of the non-AGS, rectangular-AGS, and circular-AGS antennas.

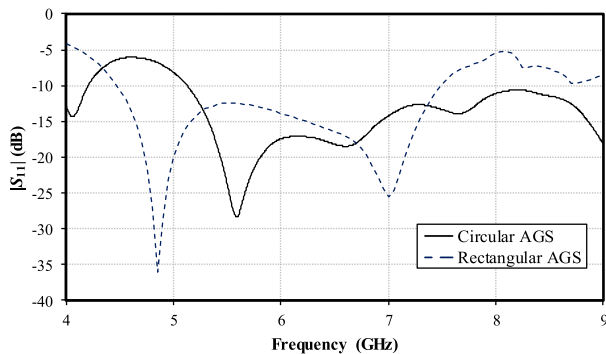


FIGURE 21. Simulated $|S_{11}|$ of the rectangular- and circular-AGS antennas.

given the corners-truncated radiating patch in Fig. 1. The AR bandwidth of the rectangular-AGS antenna is 21%, vis-à-vis 13% of the non-AGS. Meanwhile, the circular-AGS antenna (given 62 mm circular ground plane) the phenomenon of phase-difference in Fig. 5 can suppresses the resonance, resulting in an AR bandwidth of 43.81% and covering the 3-dB AR frequency band of 5.42 - 8.17 GHz.

IV. RECTANGULAR- AND CIRCULAR-AGS ANTENNAS

Fig. 21 compares the simulated $|S_{11}|$ of the rectangular-AGS [24]-[25] and circular-AGS antennas. The circular-AGS antenna (given 62 mm circular ground plane) is based on the Antenna #1 structure. The impedance bandwidths of the rectangular- and circular-AGS antenna ($|S_{11}| \leq -10\text{dB}$) are in the 4.52 - 7.42 GHz and 5.21 - 9.00 GHz frequency ranges, respectively. The impedance bandwidth is enhanced by more than 8% under the circular-AGS scheme.

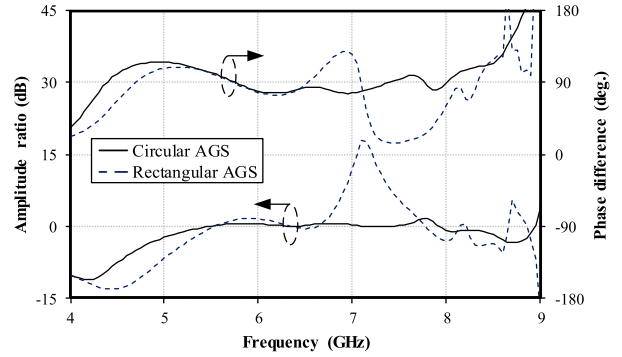


FIGURE 22. Simulated amplitude ratio and phase difference of the rectangular- and circular-AGS antennas.

Fig. 22 illustrates the simulated amplitude ratio and phase difference of the rectangular- and circular-AGS antennas. The amplitude ratio and phase difference of the circular-AGS antenna approach 0 dB and 90°, resulting in circular polarization ($AR \leq 3\text{dB}$).

Unlike the rectangular AGS, the amplitude ratio and phase difference of the circular AGS, given 62 mm circular ground plane, exhibit no resonance at 7 GHz, which is advantageous to wideband CP antenna design. The suppressed resonance is attributable to partially cut unit cells along the circular contour (Fig. 4), and the circular AGS results in a wide AR bandwidth of 6 - 9 GHz (Fig. 5).

Fig. 23 compares the simulated gains at the +z direction of the rectangular- and circular-AGS antennas. The maximum gains of the rectangular- and circular-AGS antennas are 6.72 and 9.25 dBic. The bandwidth of 3-dB gain variation of the rectangular- and circular-AGS antennas are 4.00 - 6.80 GHz (51.58%) and 3.85 - 7.00 GHz (58.06%), respectively.

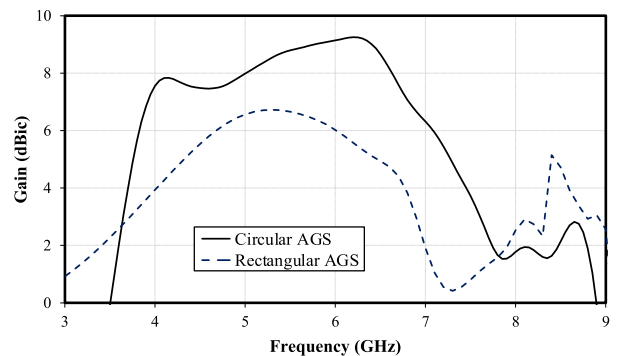


FIGURE 23. Simulated antenna gains in the +z direction of the rectangular- and circular-AGS antennas.

Fig. 24 compares the simulated co- and cross-polarization radiation patterns in the xz- and yz-planes of the rectangular- and circular-AGS antennas at 6 GHz, given the fact that the rectangular-AGS antenna failed to achieve RHCP at 7 GHz. The difference between the co- and cross-polarization is 15 dB due to high cross-polarization which is attributable

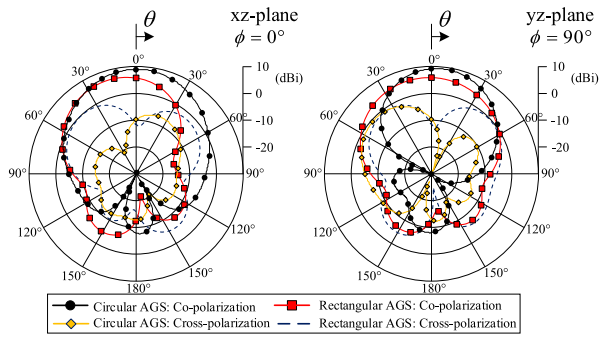


FIGURE 24. Simulated co- and cross-polarization radiation patterns in the xz- and yz-planes, at 6 GHz, of the rectangular- and circular-AGS antennas.

to the meandering probe [27], [28]. The front-to-back (F/B) ratios of the rectangular- and circular-AGS antennas are 18.76 and 16.03 dB. Despite the lower F/B ratio, the circular-AGS antenna could achieve a wider AR bandwidth (42%), compared to 21% of the rectangular-AGS antenna.

V. RESULTS AND DISCUSSION

To verify, a prototype of Antenna #1 is fabricated, and experiments undertaken. Fig. 25 illustrates the prototype of the broadband circularly polarized microstrip patch antenna with the circular AGS and meandering probe. The fabrication of the antenna and the AGS was independently carried out using RT/Duroid 5880 dielectric substrates.

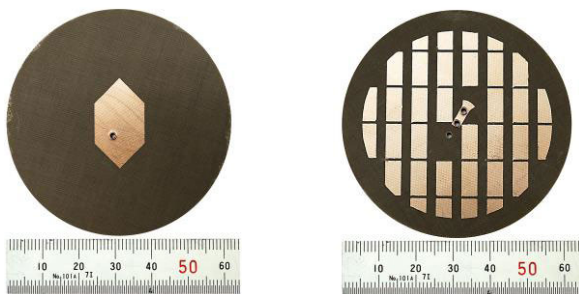


FIGURE 25. Prototype of Antenna #1: (a) the radiation layer, (b) the AGS layer.

Fig. 26 compares the simulated and measured $|S_{11}|$ of the rectangular- and circular-AGS antennas. The simulated and measured impedance bandwidths ($|S_{11}| \leq -10$ dB) are over 54% and 47.82% in the 5.12-9 GHz and 5.17-8.42 GHz frequency ranges, respectively.

Figs. 27(a)-(b) respectively illustrate the simulated and measured amplitude ratio and phase difference and AR in the +z direction of the circular-AGS antenna. The amplitude ratio and phase difference of the circular-AGS antenna is described above as in Fig. 5, for 5.5 - 8.0 GHz, vacillate around 0 dB and 90° (Fig. 27(a)). Thus, circular polarization ($AR \leq 3$ dB) could be achieved in a broadband frequency range of 5.24 - 8.17 GHz (43.81%) in the +z direction.

Figs. 28(a)-(e) respectively depict the simulated and measured co- and cross-polarization radiation patterns in the

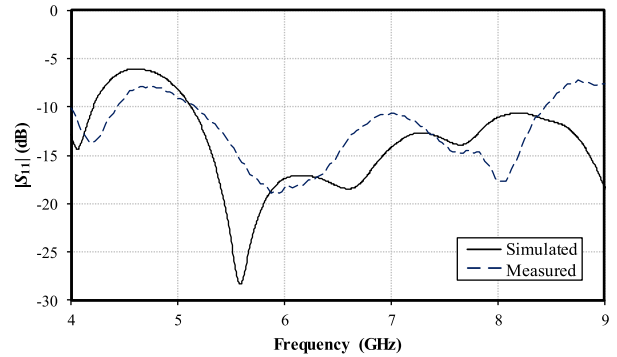
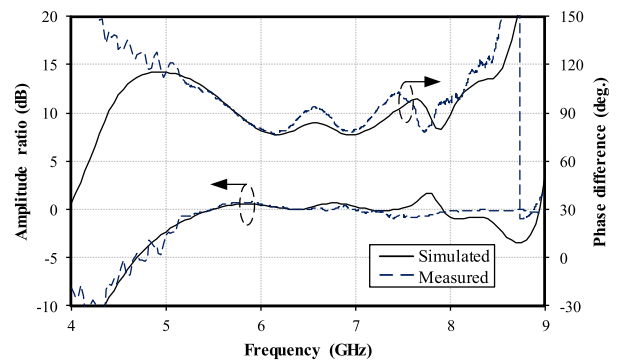
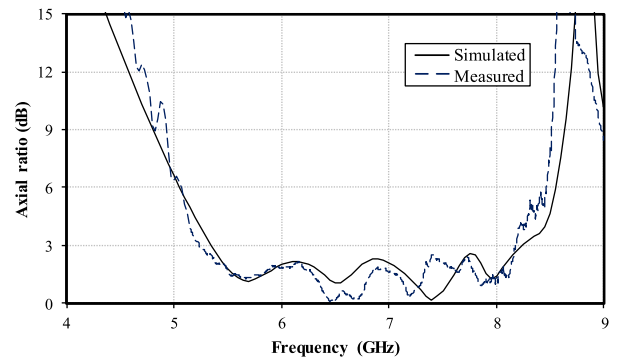


FIGURE 26. Simulated and experimental $|S_{11}|$ of the proposed circular-AGS antenna.



(a)



(b)

FIGURE 27. Simulated and measured results of the proposed circular-AGS antenna: (a) amplitude ratio and phase difference, (b) AR in the +z direction.

xz- and yz-planes of the circular-AGS antenna at 5.5, 6.0, 7.0, 7.2, and 8.0 GHz, given 62 mm circular ground plane. The xz- and yz-plane main beam of the circular-AGS antenna are slightly tilted due to the asymmetrical feeding position (Fig. 1). The simulated and measured radiation patterns are in good agreement. Fig. 29 illustrates the simulated and measured gains in the +z direction of the circular-AGS antenna. The simulation and measured results are in good agreement, with the respective maximum gains of 9.25 and 9.74 dBi. The simulated and measured bandwidth of 3-dB gain variation of the CP antenna with metasurface are 3.85 - 7.00 GHz

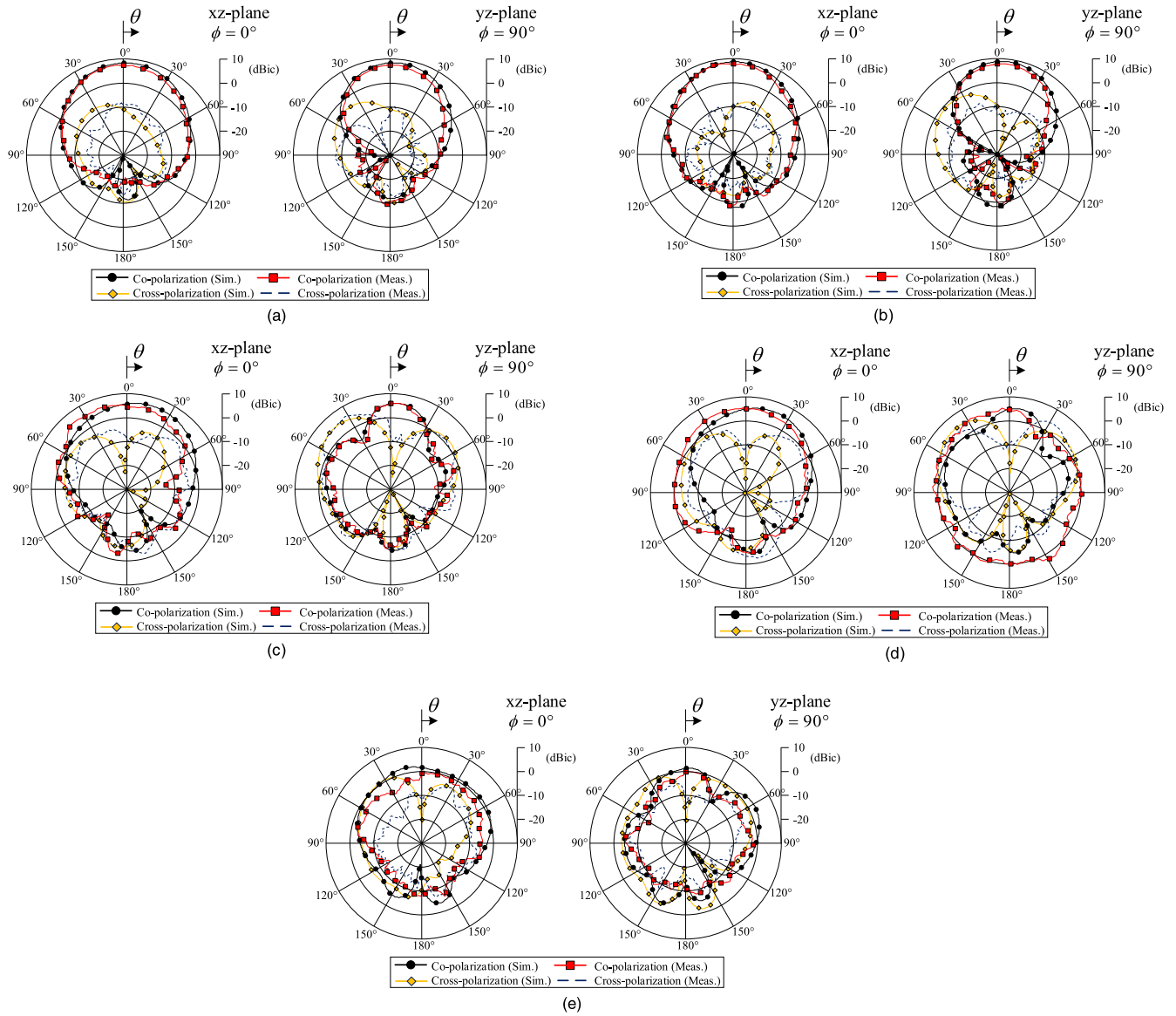


FIGURE 28. Simulated and experimental co- and cross-polarization radiation patterns in the xz- and yz-planes of the circular-AGS antenna: (a) 5.5 GHz, (b) 6.0 GHz, (c) 7.0 GHz, (d) 7.2 GHz, (e) 8 GHz.

TABLE 2. Simulated and Measured Radiation Characteristics of The Proposed CP Microstrip Patch Antenna with Circular AGS and Meandering Probe.

Frequency (GHz)	XPL (dB)				F/B Ratio (dB)				HPBW (deg.)			
	xz-plane		yz-plane		xz-plane		yz-plane		xz-plane		yz-plane	
	Sim.	Meas.	Sim.	Meas.	Sim.	Meas.	Sim.	Meas.	Sim.	Meas.	Sim.	Meas.
5.5	-19.66	-16.54	-19.66	-17.51	17.16	21.48	17.24	17.47	68.1	57.5	58.0	50.0
6.0	-18.85	-16.46	-18.85	-19.38	16.03	17.48	16.14	16.41	64.2	57.5	54.0	52.5
7.0	-18.35	-13.68	-18.35	-14.33	9.37	12.78	8.84	10.70	86.7	70.0	100.0	75.0
7.2	-22.64	-15.54	-22.64	-14.78	9.50	8.64	9.59	8.61	83.5	87.5	92.8	120.0
8.0	-21.95	-12.18	-21.95	-13.97	12.53	8.25	12.95	10.96	104.5	67.5	47.6	37.5

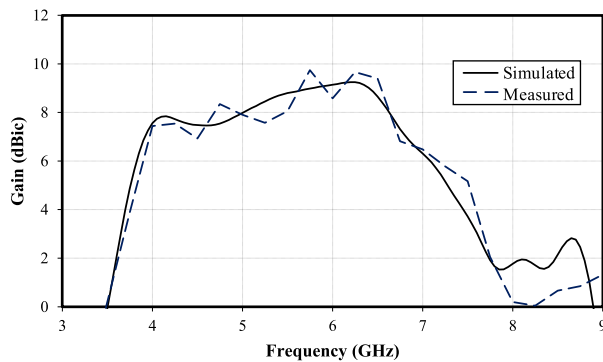
(58.06%) and 3.75 - 7.00 GHz (60.47%). The rapid fall in the broadside gain after 6.5 GHz is observed. This is due to the tilted beam direction and large side lobes caused by the higher order resonances of surface wave at high frequency. This antenna behavior is similar to that in the previous work [18].

Table 2 summarizes the simulated and measured radiation characteristics of the proposed CP microstrip patch antenna with circular AGS and meandering probe. Table 3 compares the performance of the proposed CP antenna with existing CP metasurface-based single-fed microstrip antennas in terms of

TABLE 3. Comparison Between Performance of The Proposed Antenna and Existing CP Single-Fed Microstrip Antennas with Metasurface.

References	$ S_{11} $ BW (%)	3-dB AR BW (%)	3-dB gain BW (%)	Maximum gain (dBic)	Overall antenna dimension
[1]	5.20	1.6	7.35	3.41	$0.288 \lambda_L \times 0.288 \lambda_L \times 0.030 \lambda_L$ at 2.47 GHz
[17]	36.20	33.2	34.78	7	$0.605 \lambda_L \times 0.504 \lambda_L \times 0.160 \lambda_L$ at 5.04 GHz
[18]	45.60	23.4	36.36	7.0 – 7.6	$0.496 \lambda_L \times 0.496 \lambda_L \times 0.048 \lambda_L$ at 4.70 GHz
[19]	35.00	22.00	38.99	7.72	$0.873 \lambda_L \times 0.655 \lambda_L \times 0.052 \lambda_L$ at 3.28 GHz
[20]	36.00	28.3	40.00	7.4	$0.682 \lambda_L \times 0.979 \lambda_L \times 0.050 \lambda_L$ at 3.32 GHz
[21]	40, 49.5	19.3, 33.8	66.67	7.4	$0.533 \lambda_L \times 0.533 \lambda_L \times 0.133 \lambda_L$ at 2.00 GHz
[22]	4.90	1.68	2.12	3.7	$0.327 \lambda_L \times 0.327 \lambda_L \times 0.028 \lambda_L$ at 2.80 GHz
[23]	8.18	3.3	N/A	5.1	$0.256 \lambda_L \times 0.256 \lambda_L \times 0.019 \lambda_L$ at 2.93 GHz
[24]	54.60	25.2	48.65	6.52	$0.607 \lambda_L \times 0.623 \lambda_L \times 0.083 \lambda_L$ at 4.67 GHz
[25]	42.00	22	32.00	7.2	$0.606 \lambda_L \times 0.621 \lambda_L \times 0.082 \lambda_L$ at 4.66 GHz
[30]	24.00	5.6	N/A	N/A	$1.080 \lambda_L \times 1.080 \lambda_L \times 0.098 \lambda_L$ at 3.25 GHz
Proposed antenna	47.82	43.81	60.47	9.74	$1.068 \lambda_L \times 1.068 \lambda_L \times 0.091 \lambda_L$ at 5.17 GHz

λ_L : the free-space wavelength corresponding to the lowest operating frequency of the antenna

**FIGURE 29.** Simulated and measured gains of the circular-AGS antenna relative to frequency.

fractional bandwidth of $|S_{11}| \leq -10$ dB, bandwidth of AR ≤ 3 dB, 3-dB gain bandwidth, maximum gain and antenna dimension. By comparison, the fractional bandwidths of $|S_{11}| \leq -10$ dB (47.82%), AR ≤ 3 dB (43.81%) and 3-dB gain variation (60.47%) of the proposed CP antenna are wider. The proposed antenna also achieves the highest maximum gain (9.74 dBic) with relatively low-profile dimensions.

VI. CONCLUSION

To achieve broader AR bandwidth, this research proposes a CP single-fed microstrip patch antenna using a circular AGS and meandering probe on the circular ground plane. The circular AGS, which is populated with rectangular unit cells and partially cut unit cells along the circular contour, is used to enhance the AR bandwidth; and the meandering probe to improve the impedance. Simulations are carried out, and an antenna prototype is fabricated and experimented. The performance of the circular-AGS antenna is also compared with that of rectangular-AGS antenna. The simulation results show that the circular-AGS antenna, given 62 mm circular ground plane, achieves broader impedance (5.12 - 9.00 GHz and 54%), AR (5.21 - 8.27 GHz and 45%) and gain bandwidths (3.85 - 7.00 GHz and 58.06%), vis-à-vis the rectangular-AGS antenna (4.50 - 7.45 GHz and 49%; 4.52 - 7.42 GHz and 21%; 4.00 - 6.80 GHz and 51.85 % for impedance, AR and gain bandwidths). The circular-AGS antenna can convert linear

polarization in the off-axial ratio band into right-hand circular polarization. The measured impedance, AR and gain bandwidths of the proposed circular-AGS antenna are 47.82% (5.17 - 8.42 GHz), 43.81% (5.42 - 8.17 GHz) and 60.47% (3.75 - 7.00 GHz). In essence, the CP single-fed microstrip patch antenna with circular AGS and meandering probe can achieve broader bandwidth and thus is ideal for broadband CP applications.

REFERENCES

- [1] K. Agarwal and A. Alphones, "RIS-based compact circularly polarized microstrip antennas," *IEEE Trans. Antennas Propag.*, vol. 61, no. 2, pp. 547–555, Feb. 2013.
- [2] J. G. Baek and K. C. Hwang, "Triple-band unidirectional circularly polarized hexagonal slot antenna with multiple L-shaped slits," *IEEE Trans. Antennas Propag.*, vol. 61, no. 9, pp. 4831–4835, Sep. 2013.
- [3] W. Yang, J. Zhou, Z. Yu, and L. Li, "Single-fed low profile broadband circularly polarized stacked patch antenna," *IEEE Trans. Antennas Propag.*, vol. 62, no. 10, pp. 5406–5410, Oct. 2014.
- [4] Y. Li, Z. Zhang, and Z. Feng, "A sequential-phase feed using a circularly polarized shorted loop structure," *IEEE Trans. Antennas Propag.*, vol. 61, no. 3, pp. 1443–1447, Mar. 2013.
- [5] S. Ye, J. Geng, X. Liang, Y. Jay Guo, and R. Jin, "A compact dual-band orthogonal circularly polarized antenna array with disparate elements," *IEEE Trans. Antennas Propag.*, vol. 63, no. 4, pp. 1359–1364, Apr. 2015.
- [6] K. Kandasamy, B. Majumder, J. Mukherjee, and K. P. Ray, "Dual-band circularly polarized split ring resonators loaded square slot antenna," *IEEE Trans. Antennas Propag.*, vol. 64, no. 8, pp. 3640–3645, Aug. 2016.
- [7] Z. Dong Wang, Y. Zeng Yin, X. Yang, and J. J. Wu, "Design of a wide-band horizontally polarized omnidirectional antenna with mutual coupling method," *IEEE Trans. Antennas Propag.*, vol. 63, no. 7, pp. 3311–3316, Jul. 2015.
- [8] R. Caso, A. Buffi, M. R. Pino, P. Nepa, and G. Manara, "A novel dual-feed slot-coupling feeding technique for circularly polarized patch arrays," *IEEE Antennas Wireless Propag. Lett.*, vol. 9, pp. 183–186, 2010.
- [9] K. Konstantinidis, A. P. Feresidis, and P. S. Hall, "Broadband sub-wavelength profile high-gain antennas based on multi-layer metasurfaces," *IEEE Trans. Antennas Propag.*, vol. 63, no. 1, pp. 423–427, Jan. 2015.
- [10] J. Y. Siddiqui, C. Saha, and Y. M. M. Antar, "Compact dual-SRR-loaded UWB monopole antenna with dual frequency and wideband notch characteristics," *IEEE Antennas Wireless Propag. Lett.*, vol. 14, pp. 100–103, 2015.
- [11] N. Nguyen-Trong, A. Piotrowski, T. Kaufmann, and C. Fumeaux, "Low-profile wideband monopolar UHF antennas for integration onto vehicles and helmets," *IEEE Trans. Antennas Propag.*, vol. 64, no. 6, pp. 2562–2568, Jun. 2016.
- [12] S.-W. Qu, C. H. Chan, and Q. Xue, "Wideband and high-gain composite cavity-backed crossed triangular bowtie dipoles for circularly polarized radiation," *IEEE Trans. Antennas Propag.*, vol. 58, no. 10, pp. 3157–3164, Oct. 2010.

- [13] L. Zhang, S. Gao, Q. Luo, P. R. Young, Q. Li, Y.-L. Geng, and R. A. Abd-Alhameed, "Single-feed ultra-wideband circularly polarized antenna with enhanced front-to-back ratio," *IEEE Trans. Antennas Propag.*, vol. 64, no. 1, pp. 355–360, Jan. 2016.
- [14] J.-Y. Li, R. Xu, X. Zhang, S.-G. Zhou, and G.-W. Yang, "A wideband high-gain cavity-backed low-profile dipole antenna," *IEEE Trans. Antennas Propag.*, vol. 64, no. 12, pp. 5465–5469, Dec. 2016.
- [15] R. Deng, Y. Mao, S. Xu, and F. Yang, "A single-layer dual-band circularly polarized reflectarray with high aperture efficiency," *IEEE Trans. Antennas Propag.*, vol. 63, no. 7, pp. 3317–3320, Jul. 2015.
- [16] R. Orr, V. Fusco, D. Zelenchuk, G. Goussetis, E. Saenz, M. Simeoni, and L. S. Drioli, "Circular polarization frequency selective surface operating in ku and ka band," *IEEE Trans. Antennas Propag.*, vol. 63, no. 11, pp. 5194–5197, Nov. 2015.
- [17] K. Agarwal and A. Alphones, "Wideband circularly polarized AMC reflector backed aperture antenna," *IEEE Trans. Antennas Propag.*, vol. 61, no. 3, pp. 1456–1461, Mar. 2013.
- [18] S. X. Ta and I. Park, "Low-profile broadband circularly polarized patch antenna using metasurface," *IEEE Trans. Antennas Propag.*, vol. 63, no. 12, pp. 5929–5934, Dec. 2015.
- [19] X. Qing and Z. N. Chen, "Metasurface-based low profile broadband circularly polarized antenna," in *Proc. IEEE Region Conf. (TENCON)*, Malaysia, India, Nov. 2017, pp. 2378–2382.
- [20] N. Nasimuddin, Z. N. Chen, and X. Qing, "Bandwidth enhancement of a single-feed circularly polarized antenna using a metasurface," *IEEE Antennas Propag. Mag.*, vol. 58, no. 2, pp. 39–46, Apr. 2016.
- [21] H. H. Tran and I. Park, "A dual-wideband circularly polarized antenna using an artificial magnetic conductor," *IEEE Antennas Wireless Propag. Lett.*, vol. 15, pp. 950–953, 2016.
- [22] Y. Dong, H. Toyao, and T. Itoh, "Design and characterization of miniaturized patch antennas loaded with complementary split-ring resonators," *IEEE Trans. Antennas Propag.*, vol. 60, no. 2, pp. 772–785, Feb. 2012.
- [23] H.-X. Xu, G.-M. Wang, J.-G. Liang, M. Q. Qi, and X. Gao, "Compact circularly polarized antennas combining meta-surfaces and strong space-filling meta-resonators," *IEEE Trans. Antennas Propag.*, vol. 61, no. 7, pp. 3442–3450, Jul. 2013.
- [24] T. Nakamura and T. Fukusako, "Broadband design of circularly polarized microstrip patch antenna using artificial ground structure with rectangular unit cells," *IEEE Trans. Antennas Propag.*, vol. 59, no. 6, pp. 2103–2110, Jun. 2011.
- [25] S. Maruyama and T. Fukusako, "An interpretative study on circularly polarized patch antenna using artificial ground structure," *IEEE Trans. Antennas Propag.*, vol. 62, no. 11, pp. 5919–5924, Nov. 2014.
- [26] T. Fukusako, R. Nobe, and S. Maruyama, "Effect of ground plane on circularly polarized microstrip antenna using artificial ground structure," in *Proc. IEEE Int. Symp. Antennas Propag.*, New York, NY, USA, Jul. 2012, pp. 8–14.
- [27] Y. Kai and T. Fukusako, "Broadband circularly polarized patch antenna with low crosspolarization using artificial ground structure," *Microw. Opt. Technol. Lett.*, vol. 60, no. 4, pp. 840–845, Apr. 2018.
- [28] H.-W. Lai and K.-M. Luk, "Design and study of wide-band patch antenna fed by meandering probe," *IEEE Trans. Antennas Propag.*, vol. 54, no. 2, pp. 564–571, Feb. 2006.
- [29] Q. Wei Lin, H. Wong, X. Yin Zhang, and H. Wah Lai, "Printed meandering probe-fed circularly polarized patch antenna with wide bandwidth," *IEEE Antennas Wireless Propag. Lett.*, vol. 13, pp. 654–657, Mar. 2014.
- [30] F. Yang and Y. Rahmat-Samii, "A low profile single dipole antenna radiating circularly polarized waves," *IEEE Trans. Antennas Propag.*, vol. 53, no. 9, pp. 3083–3086, Sep. 2005.



ARNON SAKONKANAPONG (Student Member, IEEE) was born in Nonthaburi, Thailand, in 1989. He received the B.Eng. and M.Eng. degrees from the King Mongkut's Institute of Technology Ladkrabang (KMITL), Bangkok, Thailand, in 2011 and 2013, respectively, where he is currently pursuing the D.Eng. degree.



RYUJI KUSE (Member, IEEE) received the B.E., M.E., and Ph.D. degrees in engineering from Fukui University, Fukui, Japan, in 2011, 2013, and 2016, respectively. In 2017, he joined Kumamoto University, Kumamoto, Japan, as an Assistant Professor, where he is currently working with the Department of Computer Science and Electrical Engineering. His research interests include meta-surface, MIMO antennas, circularly polarized antennas, and their applications. He is a member of IEICE.



CHUWONG PHONGCHAROENPANICH (Member, IEEE) received the B.Eng. (Hons.), M.Eng., and D.Eng. degrees from the King Mongkut's Institute of Technology Ladkrabang (KMITL), Bangkok, Thailand, in 1996, 1998, and 2001, respectively. He is currently an Associate Professor with the Department of Telecommunications Engineering, KMITL, where he also serves as the Leader of the Innovative Antenna and Electromagnetic Applications Research Laboratory. His

research interests include antenna design for various mobile and wireless communications, conformal antennas, and array antenna theory. He is also a member of IEICE and ECTI. He has served as the Chair of the IEEE MTT/AP/ED Thailand Chapter from 2014 to 2018. He has been on organizing committee of several international conferences, including the TPC Chair of 2009 International Symposium on Antennas and Propagation (ISAP 2009) and a TPC member of ISAP 2012. He is also a Reviewer of many scientific journals, including the IEEE TRANSACTIONS ON ANTENNAS AND PROPAGATION, IEEE ACCESS, *IET Microwaves, Antennas and Propagation, Electronics Letters*, and *ECTI Transactions*, and many international conferences, including ISAP and APMC. He was on the Board Committee of ECTI Association, from 2008 to 2011 and 2014 to 2015. He was an Associate Editor of the *IEICE Transactions on Communications* and the *ECTI Transactions on Electrical Engineering, Electronics, and Communications*. He is also an Associate Editor of the *IEICE Communications Express*.



TAKESHI FUKUSAKO (Senior Member, IEEE) received the B.E., M.E., and Ph.D. degrees in engineering from the Kyoto Institute of Technology, Kyoto, Japan, in 1992, 1994, and 1997, respectively. In 1997, he joined Kumamoto University, Kumamoto, Japan, as a Research Associate, where he is currently working as a Professor with the Department of Computer Science and Electrical Engineering. From 2005 to 2006, he was a Visiting Researcher with the University of Manitoba, MN,

Canada. He was a Visiting Associate Professor with the City University of Hong Kong, Hong Kong, SAR, China, from March 2015 to April 2015. His current research interests include antenna design, especially broadband antennas, circularly polarized antennas, and electrically small antennas, and their applications. He is a Senior Member of IEICE. In 2014, he served as one of the TPC co-chairs at the 2014 IEEE International Workshop on Electromagnetics: Applications and Student Innovation Competition (iWEM2014), and in 2017, he served as one of the general chairs of IEEE International Conference on Computational Electromagnetics (ICCEM2017). He has served as an Associate Editor for the *IEICE Transactions on Communications* from 2012 to 2016. He has been an Associate Editor of the IEEE TRANSACTIONS ON ANTENNAS PROPAGATION since 2015.

• • •



KHANET POOKKAPUND (Member, IEEE) was born in Chiangmai, Thailand, in 1989. He received the B.Eng. degree from the Rajamangala University of Technology Thanyaburi (RMUTT), in 2012, and the M.Eng. degree from the King Mongkut's Institute of Technology Ladkrabang (KMITL), Bangkok, Thailand, in 2015, where he is currently pursuing the D.Eng. degree.